

# Hadron collisions at ultrahigh energies: black disk or resonant disk modes?

V.V. Anisovich<sup>+</sup>, V.A. Nikonov<sup>+◇</sup> and J. Nyiri<sup>\*</sup>

December 6, 2024

<sup>+</sup>*National Research Centre "Kurchatov Institute", Petersburg Nuclear Physics Institute, Gatchina, 188300, Russia*

<sup>◇</sup>*Helmholtz-Institut für Strahlen- und Kernphysik, Universität Bonn, Germany*

<sup>\*</sup>*Institute for Particle and Nuclear Physics, Wigner RCP, Budapest 1121, Hungary*

## Abstract

The analysis of current ultrahigh energy data for hadronic total cross sections and diffractive scattering cross sections points to a steady growth of the optical density with energy for elastic scattering amplitudes in the impact parameter space,  $b$ . At LHC energy the profile function of the  $pp$ -scattering amplitude,  $T(b)$ , reaches the black disk limit at small  $b$ . Two scenarios are possible at larger energies,  $\sqrt{s} \gtrsim 100$  TeV. First, the profile function gets frozen in the black disk limit,  $T(b) \simeq 1$  while the radius of the black disk  $R_{black\ disk}$  is increasing with  $\sqrt{s}$ , providing  $\sigma_{tot} \sim \ln^2 s$ ,  $\sigma_{el} \sim \ln^2 s$ ,  $\sigma_{inel} \sim \ln^2 s$ . In another scenario the profile function continues to grow at  $\sqrt{s} \gtrsim 100$  TeV approaching the maximal value,  $T(b) \simeq 2$ , that means the resonant disk mode. We discuss features of the resonant disk mode when the disk radius,  $R_{resonant\ disk}$ , increases providing the growth of the total and elastic cross sections  $\sigma_{tot} \sim \ln^2 s$ ,  $\sigma_{el} \sim \ln^2 s$ , but a more slow increase of inelastic cross section,  $\sigma_{inel} \sim \ln s$ .

PACS: 13.85.Lg 13.75.Cs 14.20.Dh

## 1 Introduction

The data [1, 2] definitely confirm the previous observations [3], namely, that the total cross sections increase steadily with energy ( $\sigma_{tot} \sim \ln^n s$  as  $1 \lesssim n \lesssim 2$ ); the steady growth is observed for  $\sigma_{el}$  and  $\sigma_{inel}$ , while the ratio  $ReA_{el}/ImA_{el}$  is small and probably decreases slowly.

Already the first indications of the cross sections growth [4] gave start to corresponding models with the supercritical pomeron [5, 6]. The concept of the power growth of cross sections ( $\sigma_{tot} \sim s^\Delta$  with  $\Delta \simeq 0.08$ ) became widely accepted in the 1980s [7, 8] and is discussed till now [9] (let us note that exceeding of the Froissart bound [10] does not violate necessarily the general constraints [11]).

It was shown in [12, 13, 14] that the power-type growth of scattering amplitudes is dumped to  $\ln^2 s$ -type within the  $s$ -channel unitarization. The black disk picture with the  $\ln^2 s$ -growth of the  $\sigma_{tot}$  and  $\sigma_{el}$  at ultrahigh energies was suggested in the Dakhno-Nikonov model [15]. The model can be considered as a realization of the Good-Walker eikonal approach [16] for a continuous set of channels. Presently, the black disk mode for hadron collisions at ultrahigh energies is discussed extensively, see, for example, [17, 18, 19, 20, 21, 22, 23, 24].

The black disk mode is usually discussed in terms of the optical density for elastic scattering amplitude. For the asymptotic regime such a presentation was carried out in [25, 26]: the cross sections  $\sigma_{tot}(pp)$ ,  $\sigma_{el}(pp)$ ,  $\sigma_{inel}(pp)$  demonstrate a maximal growth,  $\sim \ln^2 s$ , while diffractive dissociation cross sections  $\sigma_D(pp)$ ,  $\sigma_{DD}(pp)$  give a slower growth,  $\sim \ln s$ .

For the calculation of screening corrections in inelastic diffractive processes at ultrahigh energies [27] the  $K$ -matrix technique is more preferable. The  $K$ -matrix function  $-iK(b)$  in the preLHC region increases with energy being mainly concentrated at  $b < 1$  fm. The black disk regime for the  $K$ -matrix function means its "freezing",  $-iK(b) \rightarrow 1$ , in the disk area. If the growth of the  $-iK(b)$  continues with increasing energy, the interaction area turns into a resonant disk. In this case asymptotically  $\sigma_{tot}(pp) \sim \ln^2 s$ ,  $\sigma_{el}(pp) \sim \ln^2 s$  with  $[\sigma_{el}(pp)/\sigma_{tot}(pp)]_{s \rightarrow \infty} \rightarrow 1$ ; the resonant disk area is surrounded by a black border band that provides  $\sigma_{inel}(pp) \sim \ln s$ ,  $\sigma_D(pp) \sim \ln s$ ,  $\sigma_{DD}(pp) \sim \ln s$ .

At present paper we perform comparative analysis of predictions for ultrahigh energy diffractive processes under these two scenarios. For resonant disk mode we consider a power growth with energy  $-iK(b) \sim s^\Delta$  but variants with a more slow growth,  $-iK(b) \sim \ln^n s$ , are possible as well.

## 2 Scattering amplitude in the impact parameter space and the $K$ -matrix representation for ultrahigh energy

In the impact parameter space the profile function  $T(b)$  is determined at high energies as:

$$\begin{aligned}\sigma_{tot} &= 2 \int d^2b T(b), \\ 4\pi \frac{d\sigma_{el}}{d\mathbf{q}_\perp^2} &= |A_{el}(\mathbf{q}_\perp^2)|^2, \quad A_{el}(\mathbf{q}_\perp^2) = i \int d^2b e^{i\mathbf{b}\mathbf{q}_\perp} T(b), \\ T(b) &= 1 - \eta(b) e^{2i\delta(b)} = 1 - e^{-\frac{1}{2}\chi(b)} = \frac{-2iK(b)}{1 - iK(b)},\end{aligned}\tag{1}$$

here  $A_{el}(\mathbf{q}_\perp^2)$  is the elastic scattering amplitude. The profile function can be presented either in the standard form using the inelasticity parameter  $\eta(b)$  and the phase shift  $\delta(b)$  or in terms of the optical density  $\chi(b)$  and the  $K$ -matrix function  $K(b)$ . The  $K$ -matrix approach is based on the separation of the elastic rescatterings in the intermediate states: the function  $K(b)$  includes only the multiparticle states thus being complex valued. The small value of the  $ReA_{el}/ImA_{el}$  tells that  $K(b)$  is dominantly imaginary.

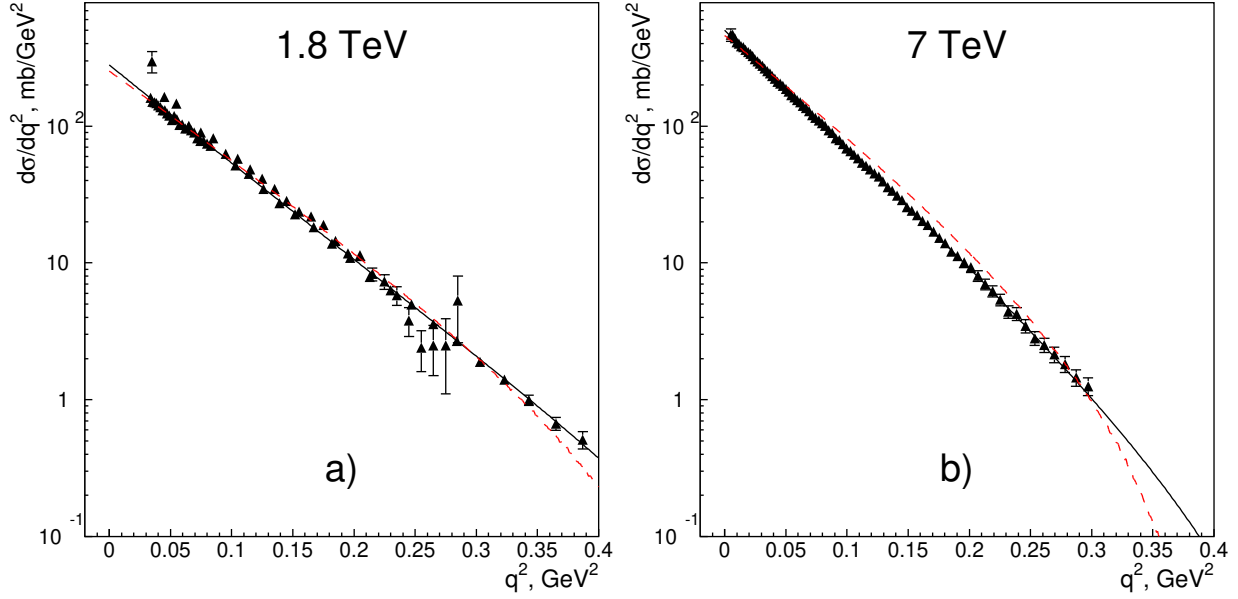


Figure 1: a,b) Differential cross sections  $d\sigma_{el}/dq_{\perp}^2$  at  $\sqrt{s} = 1.8, 7.0$  TeV and their description within the black disk mode (red dashed lines) and the resonant disk mode (solid lines).

### 2.0.1 Black disk limit in terms of the Dakhno-Nikonov model

The Dakhno-Nikonov model [15] demonstrates us a representative example of application of the optical density technique for the consideration of  $pp^{\pm}$  collisions at ultrahigh energies when  $\ln s \gg 1$ . In the model the black disk is formed by the low density pomeron cloud and rescatterings are described within the eikonal approach. The scattering amplitude  $AB \rightarrow AB$  reads:

$$A_{AB \rightarrow AB}(\mathbf{q}^2) = i \int d^2b e^{i\mathbf{q}\mathbf{b}} \int dr' \varphi_A^2(r') dr'' \varphi_B^2(r'') \left[ 1 - \exp \left( -\frac{1}{2} \chi_{AB}(r', r'', \mathbf{b}) \right) \right], \quad (2)$$

where  $dr \varphi_A^2(r)$ ,  $dr \varphi_B^2(r)$  are the quark densities of the colliding hadrons in the impact parameter space. Proton and pion quark densities can be determined using the corresponding form factors. The optical density  $\chi_{AB}(r', r'', \mathbf{b})$  depends on parameters of the  $t$ -channel interaction.

The behavior of amplitudes at ultrahigh energies is determined by leading complex- $j$  singularities, in the Dakhno-Nikonov model that are leading and next-to-leading pomerons with trajectories  $\alpha(\mathbf{q}^2) \simeq 1 + \Delta - \alpha' \mathbf{q}^2$ . The fit of refs. [22, 25] gives:

parameters	leading pole	next-to-leading
$\Delta$	0.27	0
$\alpha'_P [(\text{GeV})^{-2}]$	0.13	0.25

(3)

In terms of the K-matrix approach the black disk mode means assumed freezing of the  $-iK(b)$  in the interaction area:

$$\begin{aligned} \left[ -iK(b) \right]_{\xi \rightarrow \infty} &\rightarrow 1 && \text{at } b < R_0 \xi, \\ \left[ -iK(b) \right]_{\xi \rightarrow \infty} &\rightarrow 0 && \text{at } b > R_0 \xi, \end{aligned} \quad (4)$$

$$\xi = \ln \frac{s}{s_R}, \quad s_R \simeq 6.4 \cdot 10^3 \text{ GeV}^2, \text{ with } R_0 \simeq 2\sqrt{\alpha' \Delta} \simeq 0.08 \text{ fm.}$$

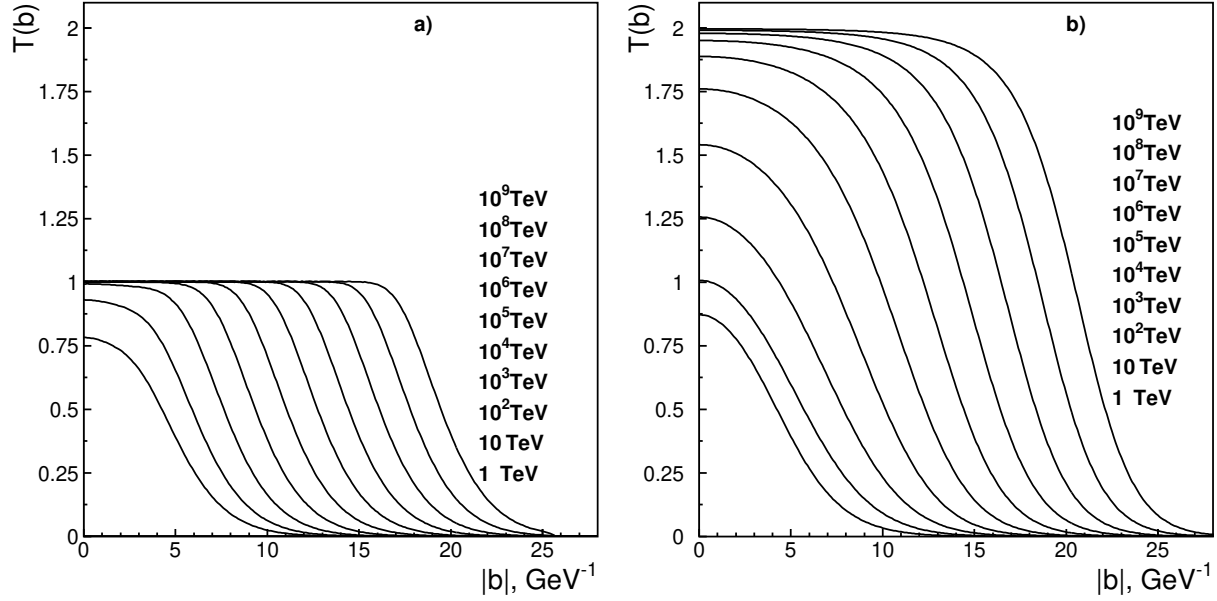


Figure 2: a) Profile functions,  $T(b)$ , at  $\sqrt{s} = 1, 10, 10^2, \dots, 10^9$  TeV for the black disk regime ( $T(b) \rightarrow 1$ ) and b) resonant disk regime ( $T(b) \rightarrow 2$ ).

The growth of the radius of the black disk is slow: small value of  $R_0$  is caused by the large mass of glueballs [28, 29] and the effective mass of gluons [30, 31].

The black disk mode results in

$$\begin{aligned}\sigma_{tot} &\simeq 2\pi(R_0\xi)^2, \\ \sigma_{el} &\simeq \pi(R_0\xi)^2, \quad \sigma_{inel} \simeq \pi(R_0\xi)^2.\end{aligned}\tag{5}$$

For the black disk radius the corrections of the order of  $\ln \xi$  exist  $R_{black\ disk} \simeq R_0\xi + \varrho \ln \xi$  but they become apparent in the Dakhno-Nikonov model at energies of the order of the Plank mass,  $\sqrt{s} \sim 10^{17}$  TeV.

### 2.0.2 Resonant disk and K-matrix function

From the data it follows that both  $T(b)$  and  $-iK(b)$  are increasing with energy, being less than unity. If the eikonal mechanism does not quench the growth, both characteristics cross the black disk limit getting  $T(b) > 1$ ,  $-iK(b) > 1$ . If  $-iK(b) \rightarrow \infty$  at  $\ln s \rightarrow \infty$ , which corresponds to a growth caused by the supercritical pomeron ( $\Delta > 0$ ), the diffractive scattering process gets to the resonant disk mode.

For following the resonant disk switch-on we use the two-pomeron model with parameters providing the description of data at 1.8 TeV and 7 TeV, namely:

$$\begin{aligned}-iK(b) &= \int \frac{d^2q}{(2\pi)^2} \exp(-i\mathbf{q}\mathbf{b}) \sum g^2 s^\Delta e^{-(a+\alpha\xi)\mathbf{q}^2} \\ &= \sum \frac{g^2}{4\pi(a+\alpha'\xi)} \exp\left[\Delta\xi - \frac{\mathbf{b}^2}{4(a+\alpha'\xi)}\right], \quad \xi = \ln \frac{s}{s_0}.\end{aligned}\tag{6}$$

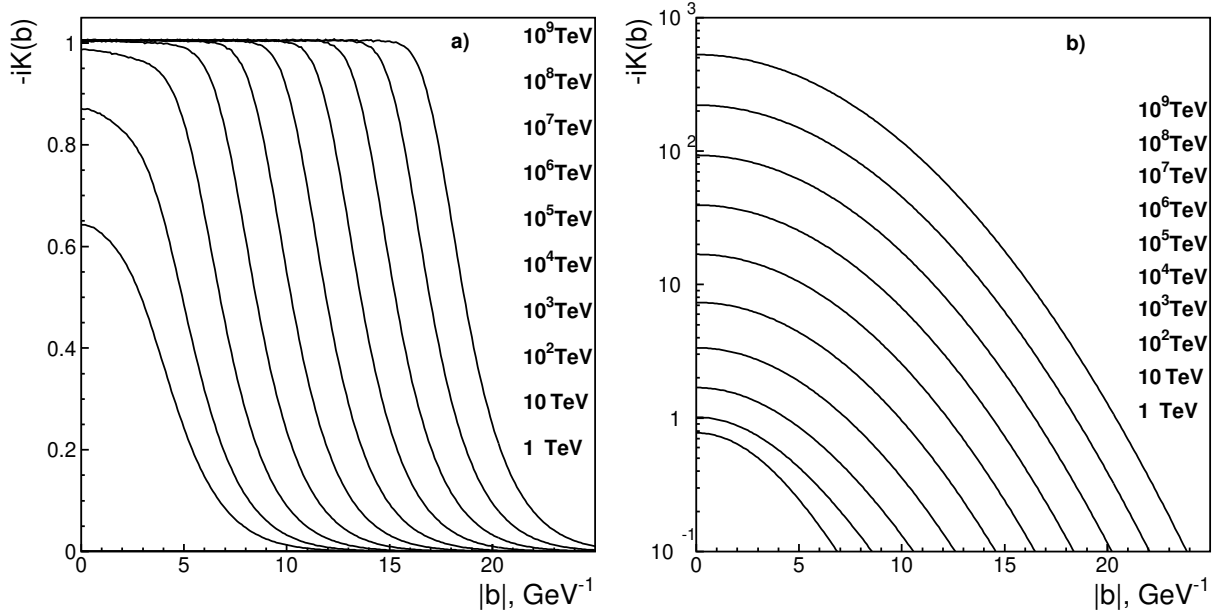


Figure 3: The K-matrix functions,  $-iK(b)$ , for a) the black disk mode ( $[-iK(b)]_{\xi \rightarrow \infty} \rightarrow 1$  at  $b < R_0\xi$ ) and b) the resonant disk mode ( $[-iK(b)]_{\xi \rightarrow \infty} \rightarrow \infty$  at  $b < R_0\xi$ ).

The following parameters are found for the leading and the next-to-leading pomerons :

parameters	leading pole	next-to-leading
$\Delta$	0.20	0
$\alpha'_P$ [GeV $^{-2}$ ]	0.18	0.14
$a$ [GeV $^{-2}$ ]	6.67	2.22
$g^2$ [ mb ]	1.74	28.6
$s_0$ [GeV $^2$ ]	1	1

(7)

The description of the differential cross sections  $d\sigma_{el}/d\mathbf{q}_\perp^2$  at  $\sqrt{s} = 1.8, 7.0$  TeV in resonant disk mode is demonstrated in Fig. 1. Resonant interaction regime occurs at  $b < 2\sqrt{\alpha'\Delta}\xi = R_0\xi$ , in this region  $T(b) \rightarrow 2$ . In terms of the inelasticity parameter and the phase shift it corresponds to  $\eta \rightarrow 1$  and  $\delta \rightarrow \pi/2$ . Cross sections at  $\xi \rightarrow \infty$  obey  $\sigma_{tot} \simeq 4\pi R_0^2\xi^2$ ,  $\sigma_{el}/\sigma_{tot} \rightarrow 1$  and  $\sigma_{inel} \simeq 2\pi R_0\xi$ .

### 2.0.3 Comparative survey of the resonant disk and black disk modes

At the energy  $\sqrt{s} \sim 10$  TeV the black cloud fills out the proper hadron domain, the region  $\leq 1$  fm, and that happens in both modes. It is demonstrated in Figs. 2,3: the profile functions  $T(b)$  coincide practically in both modes as well as the K-functions  $-iK(b)$ . Correspondingly, the differential cross sections in  $\tau$ -representation differ a little, mainly at  $\tau \sim 10$ , Fig. 4. The energy behavior of  $\sigma_{tot}$ ,  $\sigma_{el}$  and  $\sigma_{inel}$  coincide also at  $\sqrt{s} \sim 1 - 100$  TeV in both modes, Fig. 5.

Differences appear at  $\sqrt{s} \sim 1000$  TeV:  $T(b) \simeq 1.5$  at  $b \lesssim 0.5$  fm and the black zone has shifted to  $b \simeq 1.0 - 1.5$  fm, Fig. 3b. With further energy increase the radius of the black band increases as  $2\sqrt{\Delta\alpha'}\xi \equiv R_{rd}\xi$ . The rate of growth in both modes is determined by the leading singularity and the fit of the data in the region  $\sqrt{s} \sim 1 - 10$  TeV gives approximately the same values of  $\Delta$  and  $\alpha'$  for both cases thus providing  $R_0 \simeq R_{rd}$ .

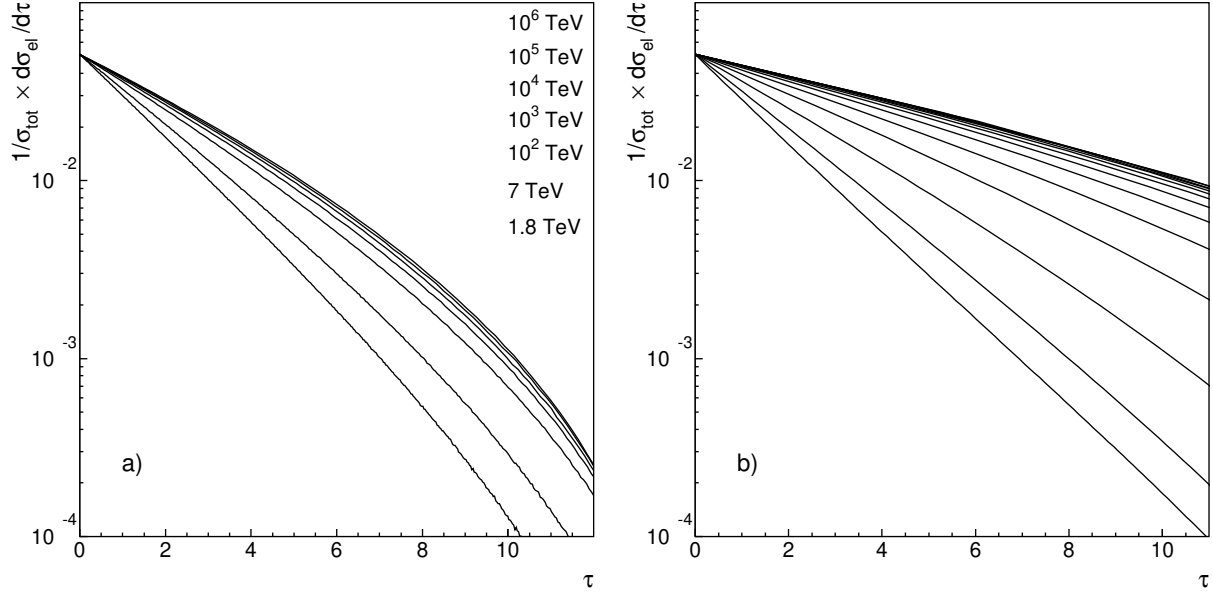


Figure 4: The  $\tau$ -representation ( $\tau = \sigma_{tot} \mathbf{q}^2$ ) for differential cross section,  $\frac{1}{\sigma_{tot}} \frac{d\sigma_{el}}{d\tau}$ , for the black disk (a) and resonant disk (b) modes.

#### 2.0.4 Logarithmic growth of the $K(b)$ -function

More slow growth of  $-iK(b)$  with energy than power, the logarithmic one, reads:

$$\begin{aligned} -iK(b) &= \int \frac{d^2q}{(2\pi)^2} \exp(-i\mathbf{q}\mathbf{b}) g^2 \xi^N \exp[-\alpha' \xi^n \mathbf{q}^2] \\ &= \frac{g^2}{4\pi\alpha'} \xi^{N-n} \exp\left[-\frac{\mathbf{b}^2}{4\alpha' \xi^n}\right], \quad \text{with } N > 0, n > 0. \end{aligned} \quad (8)$$

For the scattering amplitude eq. (8) gives:

$$\begin{aligned} A_{el}(\mathbf{q}^2) &= 2 \int d^2b e^{i\mathbf{b}\mathbf{q}} \frac{K(b)}{1 - iK(b)} \\ &= 2i\xi^n \int d^2\beta e^{i\beta\kappa} \frac{\frac{g^2}{4\pi\alpha'} \xi^{N-n} \exp[-\frac{\beta^2}{4\alpha'}]}{1 + \frac{g^2}{4\pi\alpha'} \xi^{N-n} \exp[-\frac{\beta^2}{4\alpha'}]}, \quad \beta = \frac{\mathbf{b}}{\xi^{n/2}}, \quad \kappa = \mathbf{q}\xi^{n/2}. \end{aligned} \quad (9)$$

At  $N - n > 0$  we have resonant disk picture. The disk radius squared increases with energy as  $R_{disk}^2 \simeq 4\alpha'(N - n)\xi^2 \ln \xi + g^2 \xi^2$  but the terms of the  $\ln \ln s$ -type are essential at  $\sqrt{s}$  of the order of the Plank mass.

## 3 Conclusion

The interaction of soft gluons determines the physics of hadrons. The effective gluons are massive and their mass is of the order of 1 GeV that is seen directly in radiative decays of heavy quarkonia [30, 31],  $\psi \rightarrow \gamma + \text{hadrons}$  and  $\Upsilon \rightarrow \gamma + \text{hadrons}$ . The effective gluon mass is determinative both for low energy physics, making possible to introduce the notion

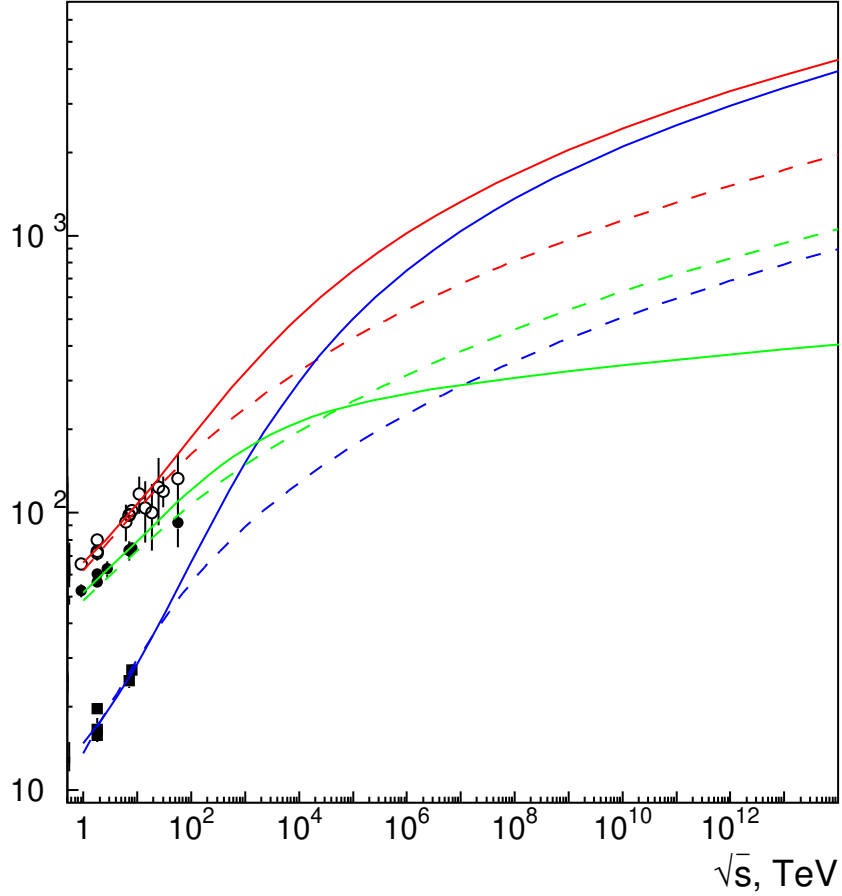


Figure 5: Total, elastic and inelastic cross sections for resonant disk (solid lines) and black disk (dashed lines) modes: red  $\sigma_{tot}$ , blue  $\sigma_{el}$ , green  $\sigma_{inel}$ .

of the constituent quark, and for high energy physics, dictating the rate of the growth of the interaction radius. High energy physics is the physics of large logarithms,  $\ln s/s_0 \gg 1$ , and the value  $\sqrt{s_0} \sim m_{effective\ gluon}$  corresponds to a start of the asymptotic regime at  $\sqrt{s} \sim 1$  TeV. However, the initial increments of the measured characteristics such as  $\sigma_{tot}$ ,  $\sigma_{el}$  and  $\sigma_{inel}$  are visually similar, and therefore their behavior in this region does not discriminate different versions. A real discrimination of modes can appear when cross section data are discussed at much larger energies,  $\sqrt{s} \sim 10^3 - 10^4$  TeV.

## References

- [1] G. Latino for the TOTEM collaboration, *Summary of Physics Results from the TOTEM Experiment*, arXiv:1302.2098(2013) [hep-ph].
- [2] Pierre Auger Collaboration (P. Abreu *et al.*), Phys. Rev. Lett. **109**, 062002 (2012).
- [3] UA4 Collaboration, Phys. Lett. **B147**, 385 (1984);  
 UA4/2 Collaboration, Phys. Lett. **B316**, 448 (1993);  
 UA1 Collaboration, Phys. Lett. **B128**, 336 (1982);

- E710 Collaboration, Phys. Lett. **B247**, 127 (1990);  
CDF Collaboration, Phys. Rev. **D50**, 5518 (1994).
- [4] Y.P. Gorin *et al.* Yad. Phys. **14**, 998 (1971).
  - [5] A. Capella and J. Kaplan, Phys. Lett. **B52**, 448 (1974).
  - [6] P.E. Volkovitsky, M.A. Lapidus, V.I. Lisin, K.A. Ter-Martirosyan, Yad. Phys. **24**, 1237 (1976).
  - [7] A. Donnachie and P.V. Landshoff, Nucl. Phys. **B231**, 189 (1984).
  - [8] A.B. Kaidalov and K.A. Ter-Martirosyan, Sov. J. Nucl. Phys. **39**, 979 (1984).
  - [9] A. Donnachie and P.V. Landshoff, arXiv:11122485, (2011) [hep-ph].
  - [10] M. Froissart, Phys. Rev. **123**, 1053 (1961).
  - [11] Y.I. Azimov, Phys. Rev. **D84**, 056012 (2011); arXiv:1208.4304(2012) [hep-ph].
  - [12] T.K. Gaisser and T. Stanev, Phys. Lett., **B219**, 375, 1989.
  - [13] M. Block, F. Halzen and B. Margolis, Phys. Lett., **B252**, 481, 1990.
  - [14] R.S. Fletcher, Phys. Rev. **D46**, 187, 1992.
  - [15] L.G. Dakhno and V.A. Nikonov, Eur. Phys. J. **A8**, 209 (1999).
  - [16] M.L. Good, W.D. Walker, Phys. Rev. **120**, 1857 (1960).
  - [17] F. Halzen, K. Igi, M. Ishida and C.S. Kim, Phys. Rev. **D85**, 074020 (2012); arXiv:1110.1479V2(2012) [hep-ph].
  - [18] V. Uzhinsky and A. Galoyan, arXiv:1111.4984v5(2012) [hep-ph].
  - [19] M.G. Ryskin, A.D. Martin and V.A. Khoze, Eur. Phys. J. **C72**, 1937(2012); arXiv:1201.6298v2(2012) [hep-ph].
  - [20] I.M. Dremin, V.A. Nechitailo, Phys. Rev. **D85**, 074009 (2012); arXiv:1202.2016 (2012) [hep-ph].
  - [21] M.M. Block and F. Halzen, Phys. Rev. **D86**, 0501504 (2013); arXiv:1208.4086v1 (2012) [hep-ph].
  - [22] V.V. Anisovich, K.V. Nikonov, and V.A. Nikonov, Phys. Rev. **D88**, 014039 (2013); [arXiv:1306.1735 [hep-ph]].
  - [23] A. Alkin, E. Martynov, O. Kovalenko and S. M. Troshin, Phys. Rev. **D89**, 091501 (2014) [arXiv:1403.8036 [hep-ph]].
  - [24] S. M. Troshin and N. E. Tyurin, Int. J. Mod. Phys. **A22**, 4437 (2007) [hep-ph/0701241].
  - [25] V.V. Anisovich, V.A. Nikonov, and J. Nyiri, Phys. Rev. **D88**, 014039 (2013); [arXiv:1310.2839 (hep-ph)].

- [26] V.V. Anisovich, K.V. Nikonov, V.A. Nikonov and J. Nyiri, Int. J. Mod. Phys. **A29**, 1450096 (2014); arXiv:1404.1904 (hep-ph).
- [27] V.V. Anisovich, M.A. Matveev, and V.A. Nikonov, *Hadron diffractive production at ultra-high energies*, arXiv:1407.4588 (hep-ph).
- [28] V.V. Anisovich, AIP Conf. Proc. **619**, 197 (2002), **717**, 441 (2004); Phys.Usp. **47**, 45 (2004), [UFN **47**, 49 (2004)].
- [29] V.V. Anisovich, M.A. Matveev, J. Nyiri, A.V. Sarantsev, Int. J. Mod. Phys. **A20**, 6327 (2005).
- [30] G. Parisi and R. Petronzio, Phys. Lett. **94**, 51 (1980).
- [31] M. Consoli and J.H. Field, Phys. Rev. **D49**, 1293 (1994).